# Time-Resolved Single Tryptophan Fluorescence in Photoactive Yellow Protein Monitors Changes in the Chromophore Structure during the Photocycle via Energy Transfer†

Harald Otto,‡ Daniel Hoersch,‡ Terry E. Meyer,§ Michael A. Cusanovich,§ and Maarten P. Heyn*,‡

*Biophysics Group, Department of Physics, Freie Universität Berlin, Arnimallee 14, 14195 Berlin, Germany, and Department of Biochemistry and Molecular Biophysics, University of Arizona, Tucson, Arizona 85721*

*Received July 22, 2005; Revised Manuscript Received October 26, 2005*

ABSTRACT: We show from time-resolved fluorescence intensity and depolarization experiments that the fluorescence of the unique tryptophan W119 of PYP is quenched by energy transfer to the 4-hydroxycinnamoyl chromophore. Whereas the intensity decay has a time constant of 0.18 ns in P, the decay in the absence of the cofactor (apo-PYP) has a single exponential lifetime of 4.8 ns. This difference in lifetime with and without acceptor can be explained quantitatively on the basis of energy transfer and the high-resolution X-ray structure of P, which allows an accurate calculation of the $\kappa^2$ factor. Fluorescence depolarization experiments with donor and acceptor indicate that both are immobilized so that $\kappa^2$ is constant on the fluorescence time scale. Using background illumination from an LED emitting at 470 nm, we measured the time-resolved fluorescence in a photostationary mixture of P and the intermediates $I_2$ and $I_2'$. The composition of the photostationary mixture depends on pH and changes from mainly $I_2$ at low pH to predominantly $I_2'$ at high pH. The $I_2/I_2'$ equilibrium is pH-dependent with a p$K_a$ of ∼6.3. In $I_2$ the lifetime increases to ∼0.82 ns. This is not due to a change in distance or to the increase in spectral overlap but is primarily a consequence of a large decrease in $\kappa^2$. $\kappa^2$ was calculated from the available X-ray structures and decreases from ∼2.7 in P to 0.27 in $I_2$. This change in $\kappa^2$ is caused by the isomerization of the acceptor, which leads to a reorientation of its transition dipole moment. We have here a rare case of the $\kappa^2$ factor dominating the change in energy transfer. The fluorescence decay in the light is pH-dependent. From an SVD analysis of the light/dark difference intensity decay at a number of pH values, we identify three species with associated lifetimes: P (0.18 ns), $I_2$ (0.82 ns), and X (0.04 ns). On the basis of the pH dependence of the amplitudes associated with $I_2$ and X, with a p$K_a$ of ∼6.3, we assign the third species to the signaling state $I_2'$. The absorption spectra of the 0.82 and 0.04 ns species were calculated from the pH dependence of their fluorescence amplitudes and of the photostationary light/dark difference absorption spectra. The $\lambda_{max}$ values of these spectra (372 and 352 nm) identify the 0.82 and 0.04 ns components with $I_2$ and $I_2'$, respectively, and validate the fluorescence data analysis. The mutant E46Q allows a further test of the energy transfer explanation, since lowering the pH in the dark leads to a bleached state with an increased spectral overlap but without the isomerization-induced decrease in $\kappa^2$. The measured lifetime of 0.04 ns is in excellent agreement with predictions based on energy transfer and the X-ray structure.

Photoactive yellow protein (PYP)[1] is a bacterial photoreceptor whose putative function is phototaxis. PYP is significant as the structural prototype of a large, diverse and important superfamily of signaling proteins which have a common motif termed the PAS domain (*1*, *2*). PAS domains are found in all kingdoms of life, generally as the sensory component of multidomain proteins. The superfamily consists of many subfamilies. The functional diversity is broad: transcriptional factors, oxygen and redox sensors, serine/threonine kinases, carboxylic acid sensors, voltage-gated potassium channels, and light sensors of bacteria and plants. Well in excess of a thousand proteins have been predicted to contain a PAS domain based on amino acid sequence alignments.

PYP is a 14 kDa cytoplasmic protein absorbing in the dark at $\lambda_{max}$ ∼ 446 nm. The chromophore is a *p*-hydroxycinnamic acid that is covalently bound to cysteine 69 via a thioester linkage. Photoexcitation initiates a photocycle which is completed in about 400 ms. A simplified version of the photocycle at neutral pH, which omits the earliest intermediates and the photoreversal reactions, is presented in Figure 1. In the initial dark state P the chromophore is trans and deprotonated with its phenolate $O^-$ hydrogen-bonded to Y42 and E46. The first long-lived intermediate is $I_1$, which is formed in several nanoseconds and decays in about 200 $\mu$s

† This work was supported by NIH Grant GM 66146 (to M.A.C.) and DFG Grants He 1382/13-1 and He 1382/14-1 (to M.P.H.).

* Corresponding author: phone, 49-30-83856160; fax, 49-30-83856299; e-mail, heyn@physik.fu-berlin.de.

‡ Freie Universität Berlin.

§ University of Arizona.

[1] Abbreviations: SVD, singular value decomposition; PYP, photoactive yellow protein; PAS domain, acronym formed from the names of the first three proteins recognized as sharing this sensory domain; LED, light emitting diode; 4HC, 4-hydroxycinnamoyl chromophore.

10.1021/bi051448l CCC: $30.25 
Published on Web 12/01/2005

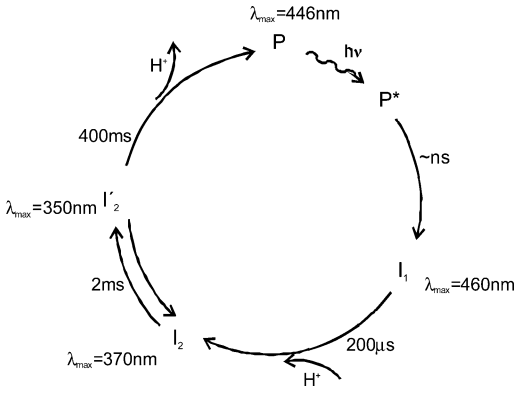


FIGURE 1: Photocycle of PYP at neutral pH. The early intermediates before $I_1$ are omitted.

to the $I_2$ intermediate. In $I_1$, the chromophore is cis and deprotonated with a red-shifted absorption maximum (465 nm). $I_2$ is the first intermediate with a protonated cis chromophore (*3*, *4*) which is blue shifted. The OH group of the chromophore is hydrogen-bonded in $I_2$ to the side chain of R52. $I_2$ decays to the signaling state $I_2'$ in about 2 ms. In solution $I_2'$ is characterized by a disordered structure (*5*), a larger radius of gyration (*6*, *7*), and a major conformational change (*6*, *8*−*10*). In $I_2'$, a hydrophobic surface area is exposed (*11*−*13*) presumably to facilitate interaction with an unknown response regulator. The cycle returns to P via the recovery step from $I_2'$.

The structure of the dark state (*14*) was obtained by high-resolution X-ray crystallography. Its structure was also determined in solution by multidimensional NMR spectroscopy (*15*). The fold of the refined average NMR structure agrees quite well with the crystal structure, with a root-mean-square deviation of 1.77 Å for the backbone of the well-defined regions (*15*). The N-terminal domain is poorly defined in the NMR solution structure.

Both cryotrapping and time-resolved methods were used to determine the structures of a number of intermediates by crystallography (*16*−*22*). The isomerization-induced changes of the 4-hydroxycinnamoyl chromophore and the binding pocket are well established. There are strong indications that the global conformational changes in $I_2'$, that are detected with solution methods, are blocked in crystals (*9*). It is thus unclear at present whether the $I_2'$ intermediate accumulates in crystals.

It has recently been shown that the photocycle is not unidirectional but that back-reactions and equilibria occur (*23*). An equilibrium between $I_1$ and $I_2$ has been detected in E46Q (*23*) and wild type (*23*−*25*). This equilibrium is pH-dependent. Photoreversal experiments demonstrated an equilibrium between $I_2$ and $I_2'$ (*26*). Recently, it was shown that the $I_1/I_2'$ equilibrium is salt-dependent and that, at low salt, the $I_2$ to $I_2'$ transition for the formation of the signaling state is blocked (*27*). It was hypothesized (*27*) that salt binds to the salt bridge K110/E12 that links the $\beta$-scaffold with the N-terminal domain (*14*, *28*). This salt bridge is presumably broken during the $I_2$ to $I_2'$ transition to facilitate detachment of the N-terminal domain from the $\beta$-sheet. A similar loss of interaction between two domains has been observed in the activation of another PAS domain photoreceptor, phototropin (*29*, *30*). In that case, the $J_\alpha$ helix detaches from the PAS core.

PYP contains a unique conserved tryptophan (W119) at the interface between the central $\beta$-sheet and the N-terminal cap. The fluorescence of this tryptophan may thus be used as a probe to monitor changes in polarity, accessibility, quenching, and dynamics during the photocycle. The hydrophobic collapse model (*2*) postulates that the signal triggered by the chromophore isomerization is propagated across the $\beta$-sheet to the N-terminal cap.

The quantum yield for fluorescence of the 4-hydroxycinnamoyl chromophore of PYP is 0.0014, very weak as expected (*31*). In the mutant Y42F, which lacks the hydrogen bond between Y42 and the chromophore oxygen, the fluorescence quantum yield is about 10 times higher (~0.018) (*32*). Steady-state emission spectra of the 4-hydroxycinnamoyl chromophore with $\lambda_{em} \sim 495$ nm were recorded with excitation at 280 nm, i.e., in the absorption band of tryptophan (*33*). These observations were interpreted as sensitized fluorescence, caused by energy transfer from the aromatic amino acids (W119 or the five tyrosines) (*33*). Since the 4-hydroxycinnamoyl chromophore also absorbs in the UV at 280 nm, direct excitation could not be excluded, however. These authors were the first to report on the fluorescence of the aromatic amino acids of PYP. The fluorescence quenching (presumably of W119) by acrylamide was reported to be stronger in a steady-state $I_2/I_2'$ mixture than in P, suggesting greater accessibility of W119 in the signaling state (*8*).

More extensive steady-state measurements on the fluorescence of W119 were recently reported (*34*). Using background illumination, the emission was also measured in a photostationary mixture of P, $I_2$, and $I_2'$. It was observed that at pH 8 the fluorescence was weaker in the $I_2/I_2'$ mixture than in P, whereas at pH 6 the opposite was the case. An approximate p$K_a$ of 6.5 was obtained. No definitive explanation for this pH effect was offered. The quantum yield for fluorescence in the dark state was found to be 0.01, unusually low for tryptophan. The authors rejected energy transfer to the 4-hydroxycinnamoyl chromophore as the major cause of quenching on the basis of the observed pH effects and since the much larger spectral overlap in $I_2/I_2'$ did not lead to the expected large reduction in fluorescence.

Here, we use time-resolved fluorescence intensity and anisotropy measurements to prove efficient energy transfer from W119 to the chromophore in P, $I_2$, and $I_2'$. We explain the pH dependence of the fluorescence lifetimes in the photostationary $I_2/I_2'$ mixture on the basis of the $I_2/I_2'$ equilibrium. The large difference in fluorescence lifetimes between P and $I_2$ reflects the change in acceptor orientation (due to the photoisomerization) and is in good agreement with current X-ray structures. The lifetime of $I_2'$ is anomalously short, suggesting an additional quenching mechanism in this structurally altered state.

## MATERIALS AND METHODS

*Protein Production and Purification.* Recombinant *Halorhodospira halophila* holo-PYP was produced by coexpression with the biosynthetic enzymes TAL and pCL and subsequently purified from *Escherichia coli* BL21(DE3) as described (*35*). The mutagenesis was performed as described (*36*). Apo-PYP was prepared according to refs *37* and *38*.

*Fluorescence Lifetime and Depolarization Experiments.* These were performed as described (*39*) by time-correlated

single-photon counting using a picosecond Ti-sapphire laser system. The instrumental response function had a width of about 70 ps at the excitation wavelength. For excitation of tryptophan at 298 nm, a frequency tripler was used. An LED emitting at 470 nm with a full width at half-maximum of 30 nm (Conrad, 10 mW) was used to generate a photostationary mixture of P and the $I_2$ and $I_2'$ intermediates in the fluorescence cuvette [3 × 3 mm, from Helma (105.251-QS)]. A UG11 band filter from Schott was used to prevent the scattered LED light from reaching the MCP detector and to block off the very weak chromophore fluorescence. A WG320 cutoff filter from Schott selected the tryptophan emission above 320 nm and blocked off scattered excitation light. Data analysis was performed by SVD analysis (see below) and the DOS version of the fitting program Globals Unlimited (http://lfd.uiuc.edu/globals/). Errors in decay times and amplitude were calculated using subroutines of Globals.

Radiationless energy transfer is well understood theoretically and well established experimentally (*40*, *41*). The rate of energy transfer $k_T$ is given by

$$k_T = (8.71 \times 10^{23})\left(\frac{J\kappa^2}{n^4 R_{DA}^6}\right)\left(\frac{\Phi_D}{\tau_D}\right) s^{-1} \quad (1)$$

$J$ is the spectral overlap integral between the emission spectrum of the donor and the absorption spectrum of the acceptor in units of $cm^3\ M^{-1}$. $\kappa^2$ is the angular factor of the interaction between the transition dipole moments of the donor ($\vec{\mu}_D$) and acceptor ($\vec{\mu}_A$). Using the angles $\alpha$, $\beta$, and $\delta$ defined in Figure 4, we have

$$\kappa^2 = (\cos\beta - 3\cos\alpha\cos\delta)^2 \quad (2)$$

Depending on the values of $\alpha$, $\beta$, and $\delta$, $\kappa^2$ varies between 0 and 4. $n$ is the index of refraction. $R_{DA}$ is the distance between the transition dipole moments of the donor and acceptor in angstroms (see Figure 4). $\tau_D$ is the fluorescence lifetime of the donor in the absence of the acceptor in seconds. $\Phi_D$ is the fluorescence quantum yield of the donor in the absence of the acceptor. According to eq 1 the rate constant for energy transfer is proportional to the product of $J$ and $\kappa^2$. A useful parameter is the Förster distance $R_0$. This is the distance at which $k_T$ equals $1/\tau_D$. Using the same units as above $R_0$ in angstroms is given by

$$R_0 = (9.78 \times 10^3)\left(\frac{J\kappa^2\Phi_D}{n^4}\right)^{1/6} \quad (3)$$

$R_0$ may be calculated for a given donor−acceptor pair if $\kappa^2$ is known.

*SVD Analysis.* SVD analysis is a mathematical method for data reduction (*42*, *43*). Let us assume that we measured fluorescence decay curves (each consisting for example of data points at 1000 discrete points in time) at 10 pH values. This defines a data matrix $I_{tp}$ with $10^4$ elements. $t$ is the time index and $p$ the pH index. Using Mathematica or a similar program package $I_{tp}$ can be factorized in a unique way in a product of three other matrices $U$, $S$, and $V$ (singular value decomposition) in the following way:

$$I_{tp} = \sum_i U_{ti}^T s_i V_{ip} \quad (4)$$

$U_{ti}^T$ are the "basis time traces" belonging to the "pH traces" $V_{ip}$, and $s_i$ are the singular values, the elements of the diagonal matrix $S$. If only two singular values are large ($s_1$ and $s_2$) and the others can be neglected, we have a large data reduction from $10^4$ to 2022: 2000 elements of $U_{t1}^T$ and $U_{t2}^T$, 20 elements of $V_{1p}$ and $V_{2p}$, and $s_1$ and $s_2$, i.e., a reduction of ≈80%. The physical background of this reduction is the interdependence of the data at the various pH values. By neglecting the contributions of the remaining smaller singular values, noise is eliminated. Let us assume that $U_{ti}^T$ can be represented (fitted) with a sum of exponentials $U_{ti}^T = \sum_j(\exp_{tj})x_{ji}$, where $\exp_{tj}$ is a single exponential time decay with decay time $\tau_j$. Then

$$I_{tp} = \sum_j \exp_{tj}\sum_i x_{ji}s_i V_{ip} = \sum_j (\exp_{tj})C_{jp} = \sum_j C_{jp}e^{-t/\tau_j} \quad (5)$$

Assigning each exponential decay to another conformation (intermediate) $j$ with different energy transfer and fluorescence lifetime $\tau_j$, we can interpret the $C_{jp}$'s as the pH-dependent relative concentrations of the conformational states $j$.

In a similar way we can decompose the matrix of the absorption spectra of a mixture of intermediates at a number of pH values $A_{\lambda p}$ ($\lambda$ is the index for the wavelength and $p$ is the index for the pH values):

$$A_{\lambda p} = \sum_i \tilde{U}_{\lambda i}^T \tilde{s}_i \tilde{V}_{ip} = d\sum_j \epsilon_{\lambda j} C_{jp} \quad (6)$$

The tilde (∼) signifies that this SVD differs from that in eq 4. $\tilde{U}_{\lambda i}^T$ is the "basis absorption spectrum" belonging to the $i$th singular value $\tilde{s}_i$, and $\tilde{V}_{ip}$ is the corresponding "pH trace". The second equality in eq 6 is simply the Lambert−Beer equation, which says that $A$ is a sum of contributions from each intermediate $j$, with $\epsilon_{\lambda j}$ its spectrum and $C_{jp}$ its concentration at the $p$th pH value. $d$ is the length of the cuvette.

If we measure the fluorescence time traces $I_{tp}$ and the absorption spectra $A_{\lambda p}$ on the same sample and at the same pH values, the intermediate concentrations $C_{jp}$ are the same, and we can use the $C_{jp}$ from the fluorescence measurements (eq 5) in eq 6 to obtain the intermediate absorption spectra using the pseudo-inverse of **C**:

$$\epsilon = (1/d)\mathbf{A}\mathbf{C}^{-1} \quad (7)$$

In eq 7 the bold symbols signify the matrices, and $\mathbf{C}^{-1}$ is constructed from the pH traces of the fluorescence experiment (eq 5).

## RESULTS

*pH Dependence of the Photostationary Equilibrium P/$I_2$/$I_2'$.* Time-resolved fluorescence measurements were performed with a photostationary mixture of intermediates. This mixture was generated by background illumination from an LED emitting at 470 nm. A 3 × 3 mm quartz fluorescence cuvette was used for these measurements with the LED mounted inside the cuvette in contact with the solution. The LED was fixed inside the cuvette in a mechanically stable way, allowing reproducible illumination conditions. To determine the composition of the photostationary mixture

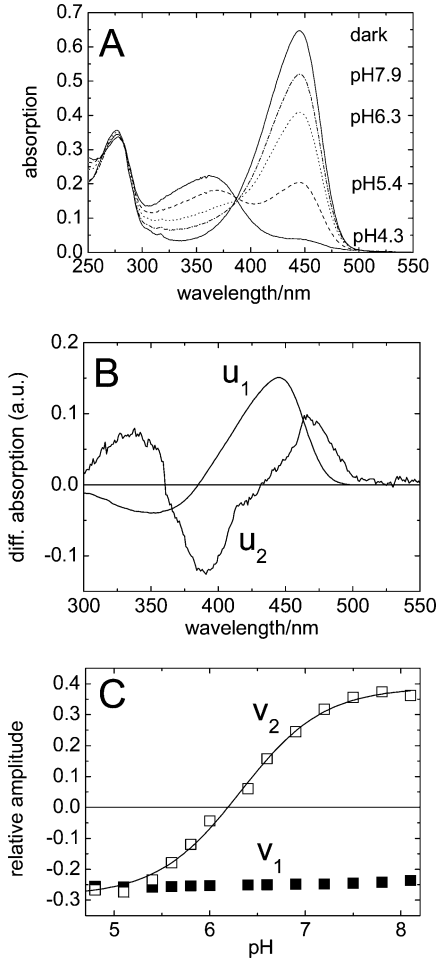


FIGURE 2: (A) pH dependence of the photostationary bleaching of PYP with a 10 mW LED emitting at 470 nm. Conditions: room temperature, 10 mM Tris, and 100 mM KCl. From top to bottom: dark spectrum and photostationary spectra at four selected pH values. (B) Basis spectra $u_1(\lambda)$ and $u_2(\lambda)$ from the SVD analysis of the normalized light − dark difference spectra from panel A. The first two singular values were 16100 and 509. (C) pH dependence of $v_1$ (■) and $v_2$ (□). The continuous solid curve is a fit to $v_2$ with the Henderson−Hasselbalch equation with p$K_a$ = 6.3 and $n$ = 1.

at each pH, the cuvette was mounted in a Shimadzu UV260 spectrometer, and the absorption spectra were measured in the dark and light. Figure 2A shows the photostationary absorption spectra at four selected pH values together with the dark spectrum. Whereas at pH 7.9 only about 20% of PYP could be bleached, this percentage rises to about 95% at pH 4. This strong pH dependence of the photostationary equilibrium between P and $I_2/I_2'$ is due to the reduction in the rate of recovery at low pH (*44*). This rate constant has a bell-shaped pH dependence with a lower p$K_a$ of approximately 6.2 and a maximum at around pH 8 (*44*). The data of Figure 2A show that, with our background illumination procedure, we can easily accumulate a large amount of $I_2/I_2'$ at low pH, but at high pH smaller amounts are accumulated. For our purposes, it is important to know the intermediate composition of the photostationary mixture at any pH. Since $I_2$ and $I_2'$ are in equilibrium (*26*), we expect that both intermediates contribute to the photostationary absorption spectra. The absorption spectra of $I_2$ and $I_2'$ are similar but not identical. Approximate spectra, presented in ref *24*, indicate that $I_2'$ is blue shifted with respect to $I_2$ by about 15−20 nm. We have analyzed the transient absorption traces of PYP at a large number of wavelengths at pH 7 and used the extrapolated difference method (*45*) to extract the spectra of $I_2$ and $I_2'$ (Borucki et al., submitted for publication). These spectra agree qualitatively with the results of ref *24* with $\lambda_{max}$ values of 350 ± 5 and 370 ± 5 nm for $I_2'$ and $I_2$, respectively. From the spectra of Figure 2A, light minus dark difference spectra were calculated at 10 pH values between 4.3 and 8.5. These difference spectra were normalized to the amount cycling and subjected to a joint SVD analysis. Only the first two singular values were significant, corresponding to two light minus dark difference spectra. The two basis spectra ($u_1$, $u_2$) and their associated pH dependencies ($v_1$, $v_2$) are shown in panels B and C of Figure 2, respectively. The dominant contribution to the light minus dark difference spectrum comes from $u_1$, which clearly reflects the P to $I_2/I_2'$ difference spectrum. This contribution is pH-independent (see $v_1$ in Figure 2C). The smaller $u_2$ contribution ($s_2/s_1 \approx 0.03$) consists mainly of a spectral blue shift of about 50 nm, which we attribute to the $I_2$ to $I_2'$ difference spectrum. The observed wavelength difference in Figure 2B between the positive peak near 340 nm and the negative peak near 390 nm is much larger than the expected true difference of about 20 nm, since the positions of the apparent extrema are pushed apart by the overlap of the positive and negative contributions from $I_2'$ and $I_2$, respectively. The $u_2$ contribution is pH-dependent [see $v_2$ (pH) in Figure 2C]. Fitting $v_2$ with the Henderson−Hasselbalch equation, we obtain a p$K_a$ of 6.3 and $n$ = 1. Below the p$K_a$ $v_2$ is negative, and accordingly the species with the higher $\lambda_{max}$ value dominates. Above the p$K_a$ $v_2$ is positive, and the species with the lower $\lambda_{max}$ dominates. On the basis of the results of ref *24* and of our photocycle studies (Borucki et al., submitted for publication) these spectral species correspond to the photocycle intermediates $I_2$ (370 nm) and $I_2'$ (350 nm). We recently showed that $I_2$ and $I_2'$ are in equilibrium (*26*). Our analysis here indicates that this equilibrium is pH-dependent with a p$K_a$ of 6.3. Note that $v_2$ is zero near pH 6.3, i.e., where the $I_2$ and $I_2'$ populations are equal. This means that $u_1$ corresponds to the P − ($I_2$ + $I_2'$) difference spectrum.

*Energy Transfer between W119 and the 4-Hydroxycinnamoyl Chromophore in P and the Photostationary Mixture of P/$I_2$/$I_2'$ at pH 4.1.* The fluorescence intensity decay curves at pH 4.1 are shown in Figure 3A in the dark (P) and in the light (photostationary state) on a logarithmic intensity scale. Under these favorable conditions, there is strong bleaching and the majority of the molecules are in the $I_2$ intermediate (Figure 2C). It is apparent from Figure 3A that the mean fluorescence lifetime is much longer in $I_2$ than in P. The decay curves for P and $I_2$ converge after a rapid decay phase to a much slower decay phase at longer times (>3 ns). This is confirmed when the decay is recorded over a longer time interval, such as 20 ns (data not shown). The third trace in Figure 3A shows the emission from apo-PYP, i.e., in the absence of the 4-hydroxycinnamoyl chromophore. This decay curve is almost a single exponential with a time constant of 4.8 ns. The light and dark decays, after 2 ns (dark trace) and 4 ns (light trace), parallel the apo-PYP decay curve. Note that the data of Figure 3A in the light and in the dark are not scaled and refer to the same sample. We conclude that the fluorescence of W119 is strongly quenched by the 4-hydroxycinnamoyl chromophore, which is about 16.3 Å away from the indole ring of W119 (*16*). The most likely

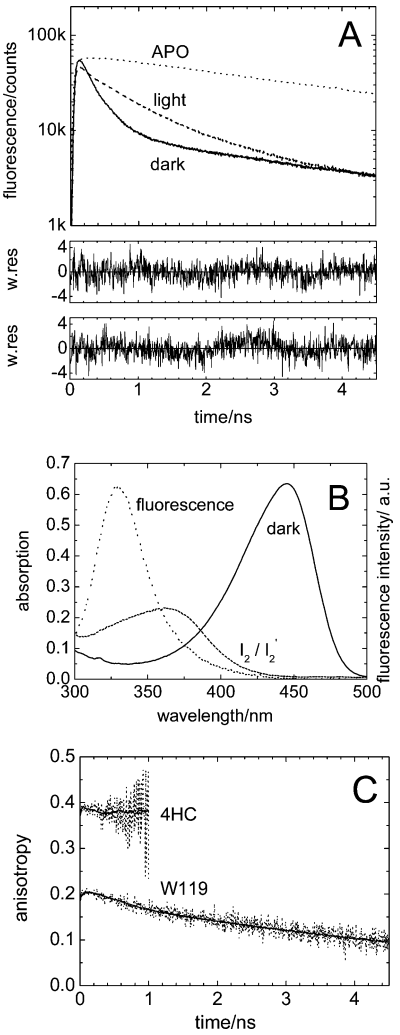


FIGURE 3: (A) Tryptophan fluorescence intensity decay curves of PYP in the dark, of PYP with background illumination with LED emitting at 470 nm (light), and of apo-PYP. Conditions: pH 4.1, room temperature, and 100 mM KCl. Excitation was at 298 nm. The weighted residuals for the dark and light decay curves are shown in the top and bottom boxes below the data points, respectively. (B) Emission spectrum of the donor W119 (- - -) and absorption spectra of the 4-hydroxycinnamoyl acceptor in the dark (P, —) and in the $I_2/I_2'$ equilibrium (•••). In the light the spectral overlap is larger than in the dark. For the numerical values of the overlap integral see Table 1. (C) Fluorescence anisotropy decay curves of W119 (lower trace) and the 4-hydroxycinnamoyl (4HC) chromophore of PYP (top trace). The 4HC chromophore was excited at 450 nm. The fitted curves correspond to a single exponential decay with a rotational correlation time of 7.8 ns.

cause of the quenching is thus energy transfer to the 4-hydroxycinnamoyl chromophore, both in P and in the photostationary mixture. An essential requirement for energy transfer is a substantial spectral overlap between the emission spectrum of the donor and the absorption spectrum of the acceptor. The emission spectrum of tryptophan 119 in the dark and the absorption spectra of the PYP chromophore in the dark and in the completely bleached form at pH 4 (mostly $I_2$) are shown in Figure 3B. The spectral overlap is clearly larger in the $I_2/I_2'$ equilibrium state than in P. Note that the emission spectrum is structureless with a maximum near 330 nm, suggesting that W119 is in a moderately hydrophobic environment and that emission occurs from the $^1L_a$ state (*40*, *47*). The numerical values of the overlap integral $J$ will be discussed below and are given in Table 1.

The decay curves of Figure 3A were deconvoluted and fitted with a sum of four exponentials. The light and dark decay curves could be fitted with the same set of exponential time constants: $\tau_1 = 0.03 \pm 0.02$ ns, $\tau_2 = 0.18 \pm 0.01$ ns, $\tau_3 = 0.83 \pm 0.03$ ns, and $\tau_4 = 4.80 \pm 0.3$ ns. The residuals for these fits are shown in the two boxes below the decay curves. The residuals are randomly distributed and indicate adequate fits. At pH 4.1 the dark state P relative amplitudes were $A_1 = 0.19 \pm 0.06$, $A_2 = 0.71 \pm 0.03$, $A_3 = 0.03 \pm 0.003$, and $A_4 = 0.07 \pm 0.007$. For the photostationary state at this pH (mostly $I_2$), the corresponding numbers are $A_1 = 0.43 \pm 0.09$, $A_2 = 0.18 \pm 0.02$, $A_3 = 0.32 \pm 0.02$, and $A_4 = 0.07 \pm 0.007$. The contribution of $\tau_4 = 4.8$ ns is the same in P and $I_2$ (7%). We attribute this contribution to a small amount of apo-PYP in the preparation. The main contribution in P is apparently from the 0.18 ns component, 71%. In the photostationary mixture, this contribution is reduced to 18%. This large decrease is consistent with the large drop in absorbance at 446 nm (Figure 2A) at this pH. The amplitude $A_3$ of the 0.83 ns component, which is virtually zero in the dark, increases by a factor of more than 10 in the photostationary state. We attribute this component to $I_2$, which is the main contributor to the photostationary mixture at this pH. The relative amplitude of the 0.03 ns component increases by a factor of more than 2 in the light. Some $I_2'$ is also present at pH 4 (see Figure 7D), and in the next section we will attribute the $A_2$ component to $I_2'$. This fastest component with $\tau_1 = 0.03$ ns is the most difficult to measure accurately with our time resolution, and the associated amplitude has a correspondingly large error.

The 4-hydroxycinnamoyl chromophore is anchored in the binding pocket in the dark in the trans configuration by three hydrogen bonds (*14*). After isomerization to the cis configuration and protonation, a new hydrogen bond is established between the hydroxyl and the side chain of R52 (*16*). We may thus expect the chromophore to be highly immobilized in P and probably also in $I_2$. Tryptophan 119 is located in the interface between the central $\beta$-sheet and N-terminal cap, and its indole chromophore is also expected to be immobilized, at least in P. Since the rate of energy transfer depends in a very sensitive way on the transition dipole moment geometry of both donor (W119) and acceptor (4-hydroxycinnamoyl) (see eqs 1 and 2), we measured the fluorescence depolarization of both to characterize their mobility on the fluorescence time scale.

These data are presented in Figure 3C for the dark state. The fluorescence anisotropy of W119 has an initial value of about 0.21 and decays with a single exponential decay time of 7.8 ns. This rotational correlation time agrees well with the calculated values of 7.4 ns for a hydrated sphere of 14 kDa tumbling in water at room temperature (*40*). This implies that no depolarization due to the motion of W119 was observable (if it occurred, it was too fast to detect). Similar data were collected for the photostationary mixture. We conclude that W119 is immobilized on the fluorescence time scale. The corresponding experiments with the 4-hydroxycinnamoyl chromophore are more difficult due to its very low fluorescence quantum yield (*31*). The very noisy data in Figure 3C for the first nanosecond clearly suggest, however, that the chromophore is also immobilized. The data beyond 1 ns are not shown because of the increasingly large fluctuations. The initial anisotropy of 0.39 is close to the

Table 1: Fluorescence Lifetimes of W119 Calculated from X-ray Diffraction Data[a]

| PDB file | intermediate | $R_{DA}$ (Å) | α (deg) | $\delta$ (deg) | $\beta$ (deg) | $\kappa^2$ | $J$ ($10^{-15}$ cm$^3$ M$^{-1}$) | $R_O$ (Å) | $\tau_{max}$ (ns) | $\tau_{min}$ (ns) |
|---|---|---|---|---|---|---|---|---|---|---|
| 1NWZ[b] | P, WT | 16.2 | 141 | 32.6 | 108 | 2.71 | 5.55 | 29.3 | 0.14 | |
| 2PYP[c] | P, WT | 16.4 | 140 | 30.3 | 110 | 2.71 | 5.55 | 29.0 | 0.15 | |
| 1OT9[d] | P, WT | 16.3 | 140 | 32.8 | 108 | 2.69 | 5.55 | 29.3 | 0.14 | |
| 2PYP[c] | $I_2$, WT | 19.0 | 88 | 29.2 | 61.7 | 0.15 | 12.7 | 20.5 | 1.92 | 1.01 |
| 1S4S[e] | $I_2$, WT | 18.4 | 93.1 | 29.4 | 68.5 | 0.26 | 12.7 | 22.7 | 1.07 | 0.63 |
| 1S4R[e] | $I_2$, WT | 18.4 | 94.5 | 30.2 | 70.6 | 0.29 | 12.7 | 23.2 | 0.98 | 0.57 |
| 1S1Y[f] | P, E46Q | 16.5 | 140 | 31.5 | 108 | 2.69 | 6.31 | 30 | 0.13 | |
| 1S1Y[f] | $I_2$, E46Q | 18.8 | 89 | 29.7 | 61 | 0.18 | 14.9 | 22 | 1.38 | |
| 1S1Y[f] | $P_{bl}$, E46Q | 16.5 | 140 | 31.5 | 108 | 2.69 | 18.8 | 35.9 | 0.05 | |
| 1T1C[g] | IL3, E46Q | 16.5 | 138 | 30.5 | 107 | 2.62 | 14.9 | 34.4 | 0.06 | |

[a] $R_{DA}$, distance between donor and acceptor transition dipole moments; α, $\beta$, and $\delta$ angles defined in Figure 4; $\kappa_2$, calculated from observed α, $\beta$, and $\delta$ according to eq 2; $J$, spectral overlap integral; $R_O$, Förster radius defined by eq 3; $\tau_{max}$ and $\tau_{min}$, upper and lower bounds of calculated lifetime of W119. [b] Reference *22*. [c] Reference *16*. [d] Reference *20*. [e] Reference *19*. [f] Reference *21*. [g] Reference *17*.

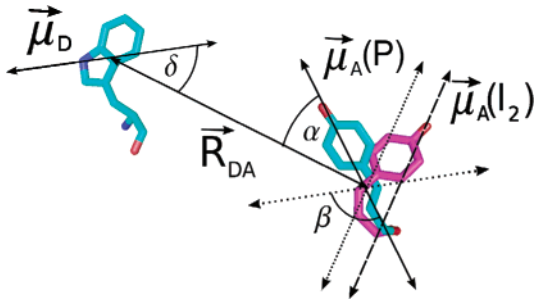


FIGURE 4: Transition dipole moment geometry of the donor ($\vec{\mu}_D$) and acceptor ($\vec{\mu}_A$) in P (blue) and $I_2$ (purple) from ref *16*. $R_{DA}$ is the vector from the donor to the acceptor. The orientations and origins of $\vec{\mu}_A$ and $\vec{\mu}_D$ in the molecular framework of the acceptor and donor are discussed in the text. For $\vec{\mu}_A(I_2)$ two positions are shown. The dashed arrow is the vector connecting the ends of the conjugated system. The dotted arrow is constructed by parallel displacement of the dashed arrow to the origin of $\vec{\mu}_A(P)$. The values of α, $\beta$, $\delta$, and $R_{DA}$ derived from the X-ray diffraction structures are listed in Table 1.

maximal value of 0.4, excluding significant motion on a faster time scale. The fit of the emission anisotropy $r(t)$ of the chromophore has the same rotational correlation time of 7.8 ns as obtained from the tryptophan data. We conclude that both the donor and the acceptor are immobilized on the fluorescence time scale. The angular factor $\kappa^2$ thus has a fixed value on the fluorescence time scale, and it is incorrect to replace it by its average value of $^2/_3$.

Fortunately, a large number of high-resolution X-ray structures are available, for P and numerous intermediates, which allow us to calculate $\kappa^2$. These structures all have well-defined geometries for the chromophore and the W119 side chain. Figure 4 shows the donor−acceptor geometry in the dark state and what is presumably the $I_2$ intermediate from PDB file 2PYP (*16*). The transition dipole moment vectors $\vec{\mu}_D$ and $\vec{\mu}_A$ are drawn fixed in the molecular planes. We excite W119 at 298 nm in the $^1L_a$ transition. The orientation of this transition dipole moment with respect to the molecular framework has been studied in detail by linear dichroism and is well established (*46*, *47*). The orientation of the indole ring of W119 does not change between P and $I_2$ in the published structures. No linear dichroism studies are available for the $S_0 \rightarrow S_1$ transition of the 4-hydroxycinnamoyl chromophore. However, based on work with related compounds (tyrosine) and other conjugated systems (various isomers of retinal), it is likely that, to a very good approximation, the transition dipole moment connects the hydroxy oxygen and the $C_9$ of the thioester, as drawn in Figure 4 [$\vec{\mu}_A(P)$]. For the origin of the transition dipole moment $\vec{\mu}_A(P)$ we chose the point halfway between $C_9$ and O. Additional evidence supporting our choice for the acceptor transition dipole moment direction will be presented in the discussion.

The angular factor $\kappa^2$ in the rate of energy transfer depends on the three angles labeled α, $\beta$, and $\delta$ in Figure 4 according to eq 2. These angles, as well as the distance $R_{DA}$ between the transition dipole moments of the donor and acceptor, were calculated from the published coordinates for various PDB files and are listed in Table 1. The chromophore orientation changes due to isomerization. For the orientation of the $S_0 \rightarrow S_1$ transition dipole moment after isomerization, we again connected the hydroxy oxygen and $C_9$ [$\vec{\mu}_A(I_2)$ in Figure 4]. For the origin of $\vec{\mu}_A(I_2)$ we chose the point halfway between $C_9$ and O, or the same origin as for $\vec{\mu}_A(P)$. These two choices are indicated by the parallel vectors (dotted arrow and dashed arrow). Note that for the choice (dashed arrow) the distance between the transition dipole moments $R_{DA}$ is about 2 Å larger in $I_2$ than in P. This is mainly due to this definition of the origin of the transition dipole moment. The center of mass of the 4HC chromophore does not change by that amount between P and $I_2$. For each structure α, $\beta$, and $\delta$ were calculated from the coordinates. $\kappa^2$ was then calculated according to eq 2, and these numbers are listed in one column of Table 1. We note that the $\kappa^2$ values are very different in P and $I_2$. For wild type, the values vary between 2.61 and 2.71 for P and between 0.15 and 0.29 for $I_2$. On the basis of $\kappa^2$ alone, energy transfer should be stronger by a factor of about 10 in P. However, there is also a large difference in the spectral overlap (Figure 3B). With maximal tryptophan emission near 330 nm, the spectral overlap is significantly larger in $I_2$ and $I_2'$ ($\lambda_{max} \sim 370$ and 350 nm, respectively) than in P ($\lambda_{max} \sim 446$ nm). The values of the spectral overlap integral $J$, determined by numerical integration, are collected in the next column. We note that the spectra for the mutant E46Q are slightly different with respect to those in wild type, so that the numbers for $J$ differ. The results show that the spectral overlap is more than twice as large in $I_2$ than in P. On the basis of $J$ alone, energy transfer should be stronger by a factor of 2.3 in $I_2$. The next column lists the values of the Förster radius calculated from $J$ and $\kappa^2$ according to eq 3 using $\Phi_D = 0.13$ (*40*) and $n = 1.39$ (*40*). We can now calculate the fluorescence lifetime from $R_O$, $R_{DA}$, and the lifetime in the absence of the acceptor (4.8 ns). Alternatively, we can calculate $k_T$ from eq 1, add to this the rate of decay in the absence of energy transfer (apo-PYP), and take the

inverse. For P, the calculated values for the structures in the first three lines of Table 1 are 0.14, 0.15, and 0.14 ns and are listed in the column $\tau_{max}$. Experimentally, we assigned the lifetime of 0.18 ns to P. The agreement is excellent. For $I_2$ (next three lines of Table 1), we either take into account the larger value of $R_{DA}$ leading to $\tau_{max}$ or use the same value for $R_{DA}$ as in P leading to $\tau_{min}$. Using these upper and lower bounds, we get ranges of 1.92−1.01, 1.07−0.63, and 0.98−0.57 ns for the three $I_2$ structures. The average values are 1.46, 0.85, and 0.77 ns. These values should be compared to the experimentally assigned lifetime of 0.83 for $I_2$. Again, the agreement is very good. Only the first value seems too large. Looking at Table 1, this deviation is due to the small value of 0.15 for $\kappa^2$ in 2PYP, compared to 0.26 and 0.29 for the other later structures 1S4S and 1S4R, which were determined by SVD methods from time-resolved crystallography. This low $\kappa^2$ value is in turn due to different values for $\alpha$, $\beta$, and $\delta$. The table shows that not all X-ray structures are equal. Our calculations show convincingly that there is quantitative agreement between the observed fluorescence lifetimes and their theoretical values based on energy transfer and the high-resolution X-ray structures of P and $I_2$. The excellent agreement strongly supports the idea that energy transfer is responsible for the shorter lifetime in P than in $I_2$. The lifetime is about 4.5 times shorter in P than in $I_2$ since the 10-fold larger $\kappa^2$ dominates over the about 2.3-fold smaller spectral overlap integral. The predominant effect is thus the isomerization-induced change in the transition dipole moment orientation of the acceptor.

Now that we have explained the different fluorescence lifetimes in P and $I_2$ by a difference in energy transfer (induced by the chromophore isomerization), the same energy transfer interpretation should also be able to explain the difference in lifetimes between P and apo-PYP. These two lifetimes are related by

$$\frac{1}{\tau_P} = \frac{1}{\tau_{apo}} + k_T = \frac{1}{\tau_{apo}}\left[1 + \left(\frac{R_0^P}{R_{DA}^P}\right)^6\right] \qquad (8)$$

With $R_0^P = 29.2$ Å and $R_{DA}^P = 16.3$ Å (the average values from Table 1), the second term on the right-hand side is 33.0 times larger than the first one. This demonstrates that energy transfer dominates all other decay processes. For the right-hand side, we get 7.2 $ns^{-1}$. For the left-hand side, we found 1/0.18 ns = 5.55 $ns^{-1}$. The agreement is very good, in particular if we consider the dependence of the right-hand side on the 6th power of $R_0^P$ and $R_{DA}^P$. We conclude that the measured lifetimes of 0.18 ns in P, 0.83 ns in $I_2$, and 4.8 ns in apo-PYP are in semiquantitative agreement with energy transfer, if we use the high-resolution X-ray structures as input for the $\kappa^2$ factor and $R_{DA}$. In the next two sections, we will describe two control experiments which provide further support for the energy transfer interpretation.

*Increasing the Overlap without a Change in $\kappa^2$: The Case of E46Q.* The structure of the mutant E46Q has also been determined to high resolution (*17*, *21*). The last four lines of Table 1 provide the structural and fluorescence parameters for E46Q. The observed values for $R_{DA}$ and $\kappa^2$ are very similar in wild type and E46Q in both P and $I_2$. In this mutant, the chromophore can be protonated in the dark without isomerization by lowering the pH below the p$K_a$ of 4.8 (*13*). So this mutant provides an opportunity to test the effect of an increase in overlap integral alone. In the inset of Figure 5A the spectra of E46Q are shown at pH 7.8 and 4.2. At the latter pH, the bleaching in the dark is almost complete. PYP is a very stable protein. Over this pH range no significant structural changes have been detected, and acid denaturation sets in with a p$K_a$ of ∼2.8 (*48*). The corresponding decay curves at the two pH values are shown in Figure 5A. Bleaching and an increase in spectral overlap lead to a shorter lifetime, as expected from energy transfer considerations. The fluorescence decay curves were measured for nine pH values ranging from 4.1 to 7.4. A global fit of all nine decay curves was possible with a common set of four lifetimes: $\tau_1 = 0.04$ ns, $\tau_2 = 0.30$ ns, $\tau_3 = 0.94$ ns, and $\tau_4 = 4.4$ ns. The longest lifetime corresponds to apo-E46Q. Its amplitude was small as for wild type and pH-independent. The same was true for the amplitude of $\tau_3$. The major amplitudes for $\tau_1$ and $\tau_2$ were strongly pH-dependent as shown in Figure 5B. The lifetime of $\tau_2 = 0.30$ ns must be assigned to the high-pH form of E46Q with the deprotonated chromophore. This value is similar to that for the dark state of wild type (0.18 ns). Our calculated value is 0.13 ns, based on 1S1Y; see Table 1. The amplitude $A_2$ is large above pH 4.8 and drops below this value. The lifetime of 0.04 ns ($\tau_1$) must be assigned to the dark bleached form with the protonated chromophore; its amplitude dominates at low pH and drops beyond pH 4.8. The solid curves in Figure 5B are simultaneous fits to the two transition curves with the Henderson−Hasselbalch equation with a p$K_a$ of ∼4.7 and a Hill coefficient of 1. Since no isomerization occurs, it is reasonable to assume that the transition dipole moment geometry in the dark bleached form is the same as in the high-pH form for which an X-ray structure is available. Using the value of the overlap integral from Table 1, we then predict a lifetime of 0.05 ns for the low-pH form of E46Q. The results of this calculation are in the line for $P_{bl}$ (dark

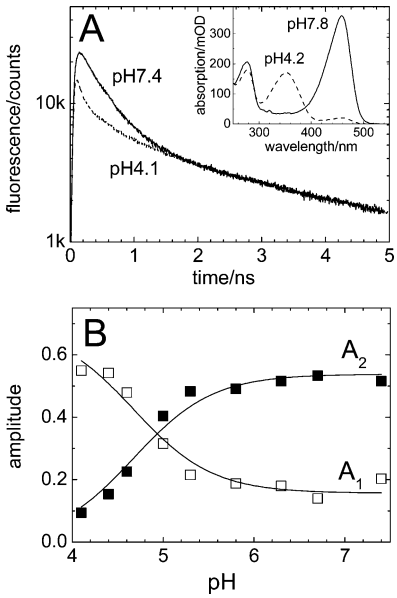


FIGURE 5: (A) Tryptophan fluorescence intensity decay curves of the mutant E46Q at pH 4.1 and 7.4. Inset: Absorption spectra of E46Q at pH 4.2 and 7.8. (B) pH dependence of the amplitude of the fastest component ($\tau_1 = 0.04$ ns, □) and the second fastest component ($\tau_2 = 0.30$ ns, ■). The continuous curves are simultaneous fits with the Henderson−Hasselbalch equation with p$K_a$ = 4.7 and $n = 1$.

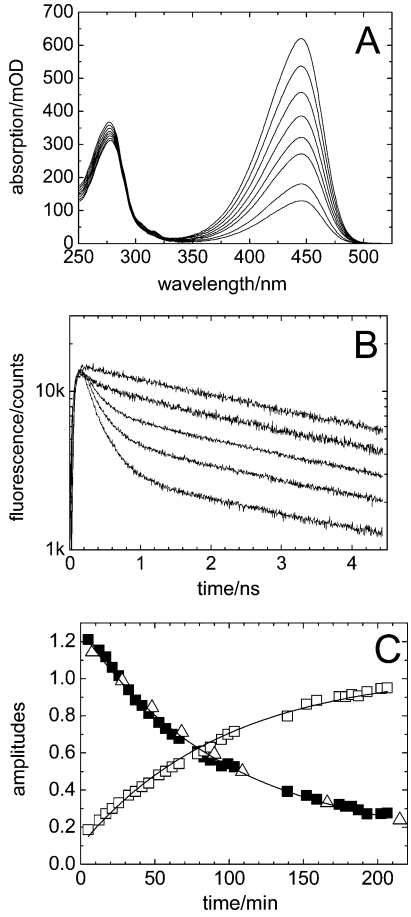


FIGURE 6: Kinetics of apo-PYP production as monitored by absorption spectroscopy of the 4-hydroxycinnamoyl chromophore (A) and fluorescence decay of tryptophan W119 (B). (A) Absorption spectra taken at times of 8, 28, 48, 68, 90, 109, 166, and 215 min after the start of the bleaching reaction (from top to bottom at 446 nm). (B) Fluorescence intensity decay curves from bottom to top at 5, 21, 46, 103, and 211 min after the start of the reaction. (C) Time dependence of the decrease in absorbance at 446 nm (Δ), of the decrease in amplitude of the fast component in the fluorescence intensity decay (■), and of the increase in the slowest component (4.8 ns) in the intensity decay (□). The solid curves are simultaneous fits to the fluorescence amplitudes (■, □) with a single exponential with $\tau = 98$ min.

bleached form of P) with structure 1S1Y in Table 1. This is in very good agreement with our observations and lends further support to the energy transfer interpretation. In the dark bleached state of E46Q the fluorescence lifetime is extremely short for two reasons: the high $\kappa^2$ factor for the trans chromophore and the high spectral overlap.

*Time Course of Bleaching Kinetics.* The removal of the chromophore is a slow chemical reaction, which takes about 4 h. It takes only a few minutes to measure a fluorescent decay curve of reasonable signal-to-noise ratio for the tryptophan fluorescence of W119. This allowed us to compare the bleaching kinetics, monitored by the loss of absorbance at 446 nm, with the kinetics of the disappearance of the fast components (from energy transfer) in the fluorescence intensity decay. The time course of the bleaching reaction for the first 215 min after starting the reaction in the measuring cuvette is shown in Figure 6A. After measurement of the absorption spectrum, the same cuvette was placed in the fluorescence spectrometer, and the decay curve was measured. Figure 6B shows a selection of 5 of the 29 decay curves. At 5 min after initiation of the reaction, the decay curve is almost indistinguishable from the "dark" decay of Figure 3A. Analysis indicates that the fast component with $\tau \approx 0.18$ ns dominates with the slowest component (4.8 ns) playing a minor role. The data of Figure 6B show that, with increasing progress of the bleaching reaction, the amplitude of the fast component decreases and that of the slow component increases. After 211 min the decay is almost single exponential with a lifetime of that of apo-PYP. At each time point the fluorescence decay curves were analyzed. The amplitudes of the fast (■) and slow (□) components are plotted in Figure 6C as a function of the reaction time. Also plotted in Figure 6C is the time dependence of the absorbance at 446 nm (△). Visual inspection of Figure 6C indicates that the kinetics of the chromophore removal (bleaching reaction) exactly parallels the kinetics of the disappearance of the fast components and of the growth of the slowest component of the fluorescence decay. This suggests that the presence of the chromophore is the cause of the fast component in the fluorescence decay curve of W119 and of the strong quenching of its fluorescence. The two fit curves represent simultaneous fits to the fluorescence amplitudes (□, ■) with a single exponential with $\tau = 98$ min.

*pH Dependence of the Fluorescence Intensity Decay in the Presence of Background Illumination.* The fluorescence decay was measured from pH 4.8 to pH 8.2 in the dark and in the $P/I_2/I_2'$ photostationary mixture produced by background illumination as described. In the dark the decay curves are virtually pH-independent (Figure 7A inset), consistent with structural stability of both the holo- and apoprotein. In the photostationary mixture of $P/I_2/I_2'$ there is a strong pH dependence. As can be discerned from Figure 7A, the amplitude of the 0.82 ns component decreases with increasing pH. In addition, changes occur in the early time range, which are also apparent in Figure 3A. To analyze these differences, we present the light/dark differences on a linear intensity scale in Figure 7B. This has several advantages. It magnifies and clarifies the early time effects which were distorted by the logarithmic scale of Figure 7A. The contribution from apo-PYP which is neither affected by light nor pH-dependent (data not shown) drops out, thereby reducing the number of species in the analysis. In this L − D difference spectrum, one recognizes three phases: two decaying components with time constants of less than 100 ps and of about 1 ns and one rising component with a time constant of perhaps 300 ps. Due to the strong overlap of the two fast components, these numbers are rough estimates. Since this is a L − D difference decay, it seems reasonable to attribute the two decaying components to $I_2'$ and $I_2$, respectively, and the rising component to P. The decrease in the 1 ns component with increasing pH is clearly due to the decrease of the $I_2$ contribution in the $P/I_2/I_2'$ mixture (see Figure 2C).

To make further progress, the combined data set (difference spectra at all 13 pH values) was subjected to SVD analysis as described in Materials and Methods. There are two significant singular values, suggesting the presence of two difference time traces: $P/I_2$ and $P/I_2'$. The corresponding two singular value time traces $u_1$ and $u_2$ are shown in Figure 7C and resemble the time traces of the difference fluorescence at pH 4.8 (mainly $I_2$) and at pH 8.1 (mainly $I_2'$),

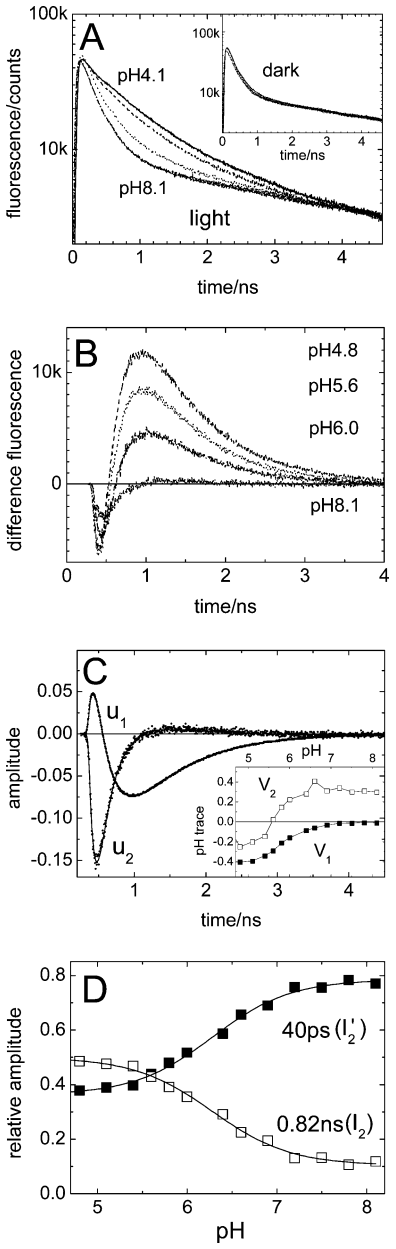


FIGURE 7: (A) pH dependence of the tryptophan 119 fluorescence decay as a function of pH in the light and in the dark (inset). The pH was varied from 4.1 to 8.1. (B) Light/dark difference intensity decay at various pH values on a linear intensity scale. (C) Time traces $u_1$ and $u_2$ for the singular values $s_1$ (388611) and $s_2$ (63702) and their common fits with three exponentials. The corresponding pH traces $v_1$ and $v_2$ are in the inset. (D) pH dependence of the amplitude of the 0.04 ns component (■) and 0.82 ns component (□) in the difference intensity of (B) normalized to the amount cycling. The solid curves represent a simultaneous fit to the data with the Henderson−Hasselbalch equation with p$K_a$ = 6.3 and $n$ = 1.

respectively (Figure 7B). $u_1$ and $u_2$ were fitted simultaneously with a sum of three exponentials (Figure 7C). The time constants were $\tau_1 = 0.04 \pm 0.02$ ns, $\tau_2 = 0.18 \pm 0.01$ ns, and $\tau_3 = 0.82 \pm 0.02$ ns. Using the pH dependence of these singular value components ($v_1$ and $v_2$, Figure 7C inset), the pH dependencies of the three time species were calculated and normalized to the amount cycling (which is itself strongly pH-dependent; see Figure 2A). This assumes that we have no other intermediates besides $I_2$ and $I_2'$ in the photostationary mixture. The pH dependencies of the amplitudes of the 0.04 ns component (■) and the 0.82 ns component (□) are presented in Figure 7D. The 0.82 ns component should be identified with $I_2$. The value of this time constant agrees well with the 0.83 ns obtained at pH 4.1 in an independent experiment (Figure 3A). The pH dependence of its amplitude (□) agrees moreover with the pH dependence of its contribution in the photostationary $I_2/I_2'$ mixture (Figure 2C). The 0.04 ns component must then, on the basis of the agreement of its pH dependence with that of $I_2'$ from Figure 2C, be identified with $I_2'$. The pH dependence of the amplitudes in Figure 7D was fitted with the Henderson−Hasselbalch equation (solid curves) leading to a p$K_a$ of about 6.3 ± 0.1, in excellent agreement with the p$K_a$ of 6.3 ± 0.06 from Figure 2C. The errors in the amplitudes of Figure 7D are considerable, since with our instrumental response function width of 70 ps, it is difficult to measure the amplitude of a 40 ps lifetime accurately. We estimate an error of 30% in this amplitude. For the 0.18 and 0.82 ns components the errors are 15% and 3%, respectively.

We conclude that the quenching of the W119 fluorescence in $I_2'$ is even stronger than in the dark state P. The spectral overlap in $I_2'$ is comparable to that in $I_2$ and thus larger than in P. The observed short lifetime of $I_2'$ could thus be due to energy transfer if it has a similarly high $\kappa^2$ value as in P. This would be the case, for example, if the chromophore would already be reisomerized in $I_2'$ (trans). However, there is no evidence for this from any of the crystallographically determined intermediate structures of wild type coming after $I_2$. The values of $\kappa^2$ for what is believed to be $I_2'$ are of the order of 0.25 and far too small to explain the 0.04 ns lifetime by energy transfer alone. This suggests that an additional quenching mechanism is operating in $I_2'$ or that the solution structure differs from the crystal structure for this intermediate.

*Absorption Spectra Associated with the Single Exponential Fluorescence Decay Species.* Using the pH dependence of the fractions ($C_i$) of the 0.04 and 0.82 ns single exponential decay species derived from the time-dependent fluorescence (Figure 7D), we can calculate their associated absorption spectra ($\epsilon_i$) from the pH dependence of the L − D difference spectra $\Delta A(\lambda,\mathrm{pH})$ of Figure 2A. This procedure was explained in detail in Materials and Methods. According to the Lambert−Beer law:

$$\Delta A(\lambda,\mathrm{pH}) = d\sum_i [\epsilon_i(\lambda) - \epsilon_p(\lambda)]C_i(\mathrm{pH}) \qquad (9)$$

With $\Delta A(\lambda,\mathrm{pH})$ from Figure 2A and $C_i$ (pH) from the lifetime components of Figure 7D we obtain the difference spectra $[\epsilon_i(\lambda) - \epsilon_p(\lambda)]$ by matrix inversion of eq *9*. The spectra associated with the 0.04 and 0.82 ns species were calculated from these difference spectra by adding an amount of $\epsilon_p$ scaled in such a way that the absorbance at 446 nm became zero. The resulting spectra for the 0.82 ns and 40 ps species are shown in Figure 8 and have $\lambda_{max}$ values at 372 and 352 nm, respectively. The spectrum of the 40 ps species is blue shifted by about 20 ns with respect to that of the 0.82 ns species. These $\lambda_{max}$ values clearly correspond to the $I_2$ and $I_2'$ photocycle intermediates (Figure 2B and ref *24*). On the basis of their absorption spectra we should thus identify the 0.04 ns species with $I_2'$ and the 0.82 ns species with $I_2$. The assignment, in the fluorescence data analysis, of the single exponential lifetimes of 0.82 and 0.04 ns to separate

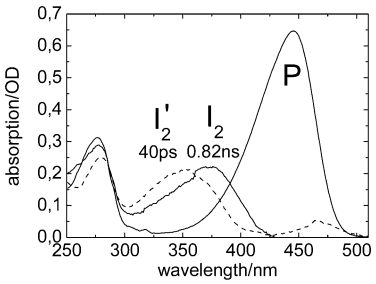


FIGURE 8: Absorption spectra of the 0.04 and 0.82 ns single exponential decay species calculated from eqs 7 and 9 using the pH dependence of the photostationary L − D difference spectra of Figure 2A and the pH dependence of the fluorescence amplitudes from Figure 7D. These spectra identify the 0.82 and 0.04 ns fluorescence decay species as the photocycle intermediates $I_2$ and $I_2'$.

structural and spectral species is thus validated by the apparent agreement between their absorption spectra derived on this basis and the absorption spectra derived from transient or photostationary absorption spectroscopy. The spectrum of $I_2'$ has a small contribution in the range 470 nm which is probably due to $I_1$. This was already apparent from the SVD basis spectrum $u_2$ of Figure 2B. This is not an artifact of the data analysis. $I_1$ is in equilibrium with $I_2$ and $I_2'$ (*23*, *27*), and a small amount of $I_1$ decays together with $I_2$ and $I_2'$ to P.

## DISCUSSION

We performed a series of experiments to show that the fluorescence of the only tryptophan of PYP, W119, is strongly quenched by energy transfer to the 4-hydroxycinnamoyl chromophore. The evidence is convincing: (1) Removal of the chromophore (apo-PYP) led to a large increase in the fluorescence lifetime of W119 (4.8 ns). The kinetics of chromophore bleaching matched the kinetics of the growth of the 4.8 ns component in the fluorescence decay curve. (2) Using the transition dipole moment geometry in the dark state P and calculating $\kappa^2$ from the high-resolution X-ray structures, there is semiquantitative agreement between the measured and calculated fluorescence lifetimes in P and apo-PYP. (3) Using the transition dipole moment geometries in P and $I_2$, derived from the X-ray structures, the observed increase in fluorescence lifetime in $I_2$ can be quantitatively explained. (4) In the mutant E46Q, an even shorter lifetime of 0.04 ns was observed at pH 4.1, when the chromophore protonates in the dark without isomerization. In this case, the large $\kappa^2$ and large spectral overlap combine to produce a very high rate of energy transfer. Quantitative agreement between observed and calculated fluorescence lifetimes was again obtained on the basis of energy transfer.

High-resolution structures are available for wild type and mutants, in the dark state and the intermediates. This allowed us to calculate accurate $\kappa^2$ factors for all states. The X-ray data suggest well-defined orientations for the indole and 4-hydroxycinnamoyl side chains with low-temperature factors. Our fluorescence depolarization experiments are in agreement, indicating immobilization of the donor and acceptor on the fluorescence time scale. We have here a rare case of the $\kappa^2$ factor dominating the change in energy transfer. From P to $I_2$, $\kappa^2$ decreases by a factor of about 10, more than compensating the increase in spectral overlap.

It is well-known that a single tryptophan residue can have multiple lifetimes (*40*). Here, we assigned each lifetime to a separate donor−acceptor conformation. The data analysis supports these assignments. This analysis has its shortcomings and limitations, however. For example, in P at pH 4.1, after correction for the apo-PYP contribution, about 80% of the amplitude is associated with the 0.18 ns lifetime. Most of the remaining 20% is associated with the 0.03 ns component. This fastest component was difficult to measure accurately with our instrumental response function of 70 ps width. That is also the reason for the large errors in this amplitude in the analysis of the $P/I_2/I_2'$ mixture. Our approach of assigning one decay time to one conformational species is validated by the spectacular agreement between the spectra of $I_2$ and $I_2'$ obtained on this basis from the fluorescence analysis and from transient and photostationary absorption spectroscopy.

Using background illumination by an LED, we were able to accumulate $I_2/I_2'$ in a photostationary state and to measure its fluorescence decay. This is a significant technical advance which will allow further experiments in $I_2$, $I_2'$, and other intermediates such as $I_1$ with different chromophore isomerization states.

An important aspect of our analysis concerns the orientation and location of the transition dipole moments in the molecular frameworks of the donor and acceptor. For the donor, this is straightforward since a large body of experimental evidence exists (*46*, *47*). We excited W119 at 298 nm, i.e., presumably in the $^1L_a$ transition. Under these conditions the fluorescence spectrum with maximal emission at 330 nm is structureless (see Figure 3B), supporting the assumption that emission occurs from $^1L_a$. For the acceptor, fewer experimental data are available. For P there are quantum chemical calculations which support our choice, with the vector connecting the hydroxyl O and $C_9$ (*49*). After isomerization around the $C_7{=}C_8$ double bond we also determined the acceptor transition dipole moment vector by connecting these atoms. This is supported by measurements of the absorption anisotropy in $I_0$ (*50*). This early intermediate has the cis configuration. The orientation of the transition dipole moment in $I_0$ (cis) differed by 24° from that in P (trans) (*50*). This is close to the angle of 17° which we calculate when we fix the transition dipole moment orientation in P and $I_0$ by the above procedure. Our assignment is thus in agreement with experimental data for $I_0$. For the isomers in the retinal proteins, similar questions have been investigated in detail (*51*−*53*). For various retinal isomers, the transition dipole moment directions were measured by linear dichroism (LD) in crystals (*52*). The results were in good agreement with the procedure described above of connecting the ends of the conjugated system (*52*). This procedure is also strongly supported by LD experiments with bacteriorhodopsin reconstituted with 3,4-dehydroretinal (*53*). In this retinal analogue the conjugation is extended into the $\beta$-ionone ring, and the transition dipole moment orientation changes in comparison with bacteriorhodopsin reconstituted with retinal by the amount predicted when the ends of the conjugated system are connected (*53*).

We found that the composition of the photostationary mixture is strongly pH-dependent. At low pH, $I_2$ dominates; at high pH, $I_2'$. A p$K_a$ of about 6.3 was obtained (Figure 2C). We recently showed that $I_2$ and $I_2'$ are in equilibrium

(*26*). We now find that this equilibrium is pH-dependent.

The pH dependence of the fluorescence decay data of the $I_2/I_2'$ mixture could also be explained on this basis provided we assigned the shortest lifetime of 0.04 ns to $I_2'$ (Figure 7D). Our time-dependent fluorescence analysis can readily explain the pH dependence of the steady-state fluorescence spectra in the photostationary state (*34*). These authors observed that at pH 8 the fluorescence in the light was smaller than in the dark, whereas at pH 6 the opposite was the case. The light minus dark difference fluorescence had a p$K_a$ of 6.5 (*34*). Since the lifetime of P (0.18 ns) lies between the lifetimes of $I_2$ (0.83 ns) and $I_2'$ (0.04 ns), the fluorescence in the light is larger when $I_2$ dominates (at low pH) and smaller when $I_2'$ dominates (at high pH). This argument can be quantified by calculating the steady-state L − D difference fluorescence by integrating the time-dependent difference intensity of Figure 7B at each pH. The difference decay was fitted with a sum of three exponentials, $\sum_i A_i e^{-t/\tau_i}$. The steady-state difference is then proportional to $\sum_i A_i \tau_i$ with $\sum_i A_i = 0$.

We can thus eliminate one $A_i$. With $\tau_1 = 0.04$ ns, $\tau_2 = 0.18$ ns, and $\tau_3 = 0.83$ ns, we have after elimination of $A_2$:

$$\sum_i A_i \tau_i = A_1(\mathrm{pH})(\tau_1 - \tau_2) + A_3(\mathrm{pH})(\tau_3 - \tau_2) \quad (10)$$

The pH dependencies of $A_1$ and $A_3$ are presented in Figure 7D and have p$K_a$'s of 6.3. The steady-state difference fluorescence predicted by eq 10 therefore also has this pH dependence and p$K_a$ and provides a quantitative explanation for the results of ref *34*. What remains unclear is to which group or residue this p$K_a$ should be assigned.

A surprising result of our investigation is the very short lifetime for $I_2'$. The simplest explanation for this number (0.04 ns) is that, in $I_2'$, the transition dipole moment direction has already returned to that of P (trans). Energy transfer would be extremely efficient due to the combination of a high $\kappa^2$ and large overlap, as in the dark low pH form of E46Q. Recently, a novel late intermediate IL3 was identified in time-resolved diffraction studies with the mutant E46Q in which the chromophore has reisomerized and adopts a chromophore structure almost identical to that of P (*17*). The structural parameters are listed in the last line of Table 1. From the values of $\alpha$, $\beta$, $\delta$, and $\kappa^2$, it is clear that the geometry is indeed very close to that of P. With $\kappa^2 = 2.62$ and $J = 14.9 \times 10^{-15}$ cm$^3$ M$^{-1}$, we calculate a fluorescence lifetime of 0.06 ns, in very good agreement with the observed value for $I_2'$ of 0.04. So far, no such late trans intermediate has been reported for wild type, however, from either crystallography or vibrational spectroscopy. It is currently believed that the reisomerization is the rate-limiting step in the recovery, making the above explanation unlikely. We showed, for example, from photoreversal experiments with double flash excitation that late $I_2'$ could be photoreversed, suggesting that $I_2'$ is cis (*26*).

An alternative explanation with a cis chromophore in $I_2'$ is suggested by the chromophore structures of the $I_1$ intermediate (*18*, *20*). In this intermediate the deprotonated cis chromophore remains in the binding pocket, the hydrogen bonds with E46 and Y42 are preserved, and the thioester part of the chromophore is flipped over by the isomerization. Consequently, the long axis of the chromophore has almost the same direction as in P. This is backed up by calculations of $\kappa^2$ based on the published structures of $I_1$ (*18*, *20*), which lead as expected to high $\kappa^2$ values of 2.9 and 2.6, respectively. The short fluorescence lifetime in $I_2'$ could thus be explained if in this intermediate the cis chromophore returned to the binding pocket with a configuration as in $I_1$, but with a protonated chromophore.

Recently, an NMR structure of what is presumably the $I_2'$ intermediate in the $\Delta$25 deletion mutant was presented (*54*). This solution structure is partially unfolded, and the 4HC chromophore is exposed at the surface with large rotational mobility. An ensemble of 20 possible $I_2'$ structures was presented in ref *54*. Could these explain the short fluorescence lifetime of $I_2'$ on the basis of energy transfer? The values of $\kappa^2$ and $R_{DA}$ in these 20 structures vary widely. Their average values are 0.4 and 29 Å, respectively. Due to the small $\kappa^2$ and large $R_{DA}$ values the rate of energy transfer is low in all structures. The average calculated fluorescence lifetime of 4.1 ns is close to that without energy transfer (apo-PYP) and more than 100 times longer than the observed value of 0.04 ns. These structures are thus not consistent with the observed fluorescence lifetime of W119 in $I_2'$ in wild type, unless additional unknown quenching mechanisms are invoked. It remains to be seen, of course, whether wild-type PYP exhibits the same large-scale unfolding as the $\Delta$25 mutant in which the N-terminal domain is missing.

Our results show that for P, $P_{bl}$ (E46Q), and $I_2$ there is excellent agreement between the observed fluorescence lifetimes in solution and their calculated values based on the structure in crystals. For $I_2'$, however, this agreement breaks down. This is in accordance with the results of other solution studies (*4*−*10*) which indicate a major conformational change in $I_2'$, which is not observed to this extent in the crystal structures. It is thus not surprising that in the partially unfolded structure of $I_2'$ additional quenching mechanisms may occur leading to the very short observed lifetime of $I_2'$. We recently suggested (*27*) that in the $I_2$ to $I_2'$ transition the salt linkage between K110 and E12 is broken, allowing the N-terminal cap to dissociate from the $\beta$-scaffold to which W119 is attached. Such a structural change would alter the environment and accessibility of W119 and affect the lifetime.

## CONCLUSIONS

We showed that the fluorescence of the unique tryptophan W119 of PYP is strongly quenched in the dark state P by energy transfer to the 4-hydroxycinnamoyl chromophore.

Using background illumination, we measured the fluorescence decay in a photostationary mixture of P and the slowest intermediates $I_2$ and $I_2'$, including the signaling state $I_2'$.

In the $I_2$ intermediate energy transfer is much reduced compared to P despite the increase in spectral overlap. The reduction in energy transfer can be quantitatively explained by a major decrease of the angular factor $\kappa^2$, which is due to the isomerization-induced orientational change of the 4-hydroxycinnamoyl chromophore.

For the dark states P and $P_{bl}$ and the intermediate $I_2$, the observed fluorescence lifetimes of W119 in solution are in excellent agreement with those calculated on the basis of the high-resolution X-ray structures in the crystalline state. Our data support the $\kappa^2$ dependence of the Förster equation

in a case where the donor and acceptor are immobilized on the fluorescence time scale and where $\kappa^2$ changes from 2.7 in P to 0.27 in $I_2$. This covers almost the entire possible range of $\kappa^2$ values.

For the $I_2'$ intermediate this agreement breaks down. This is probably due to the fact that the major conformational change that is observed in $I_2'$ in solution is blocked in the crystalline state.

Using SVD methods, we could assign absorption spectra to the fluorescence lifetime species associated with $I_2$ and $I_2'$. These spectra have their maxima at 372 and 352 nm for $I_2$ and $I_2'$, respectively.

From the pH dependence of the time-resolved fluorescence and of the steady-state absorbance in the $I_2$/ $I_2'$ photostationary state, we find that the $I_2/I_2'$ equilibrium is pH-dependent with a p$K_a$ of ≈6.3. Below this p$K_a$ $I_2$ dominates.

## ACKNOWLEDGMENT

We thank Berthold Borucki and Chandra Joshi for helpful discussions and Elsa Chan and Marion Badow for technical support.

## REFERENCES

1. Taylor, B. L., and Zhulin, I. B. (1999) PAS domains: Internal sensors of oxygen, redox potential, and light, *Microbiol. Mol. Rev. 63*, 479−506.
2. Cusanovich, M. A., and Meyer, T. E. (2003) Photoactive yellow protein: A prototypic PAS domain sensory protein and development of a common signaling mechanism, *Biochemistry 42*, 4759−4770.
3. Unno, M., Kumauchi, M., Sasaki, J., Tokunaga, F., and Yamauchi, S. (2000) Evidence for a protonated and cis configuration chromophore in the photobleached intermediate of photoactive yellow protein, *J. Am. Chem. Soc. 122*, 4233−4234.
4. Pan, D., Philip, A., Hoff, W. D., and Mathies, R. A. (2004) Time-resolved resonance Raman structural studies of the pB′ intermediate in the photocycle of photoactive yellow protein, *Biophys. J. 86*, 2374−2383.
5. Rubinstenn, G., Vuister, G. W., Mulder, F. A. A., Dux, P. E., Boelens, R., Hellingwerf, K. J., and Kaptein, R. (1998) Structural and dynamic changes of photoactive yellow protein during its photocycle in solution, *Nat. Struct. Biol. 5*, 568−570.
6. Sasaki, J., Kumauchi, M., Hamada, N., Oka, T., and Tokunaga, F. (2002) Light-induced unfolding of photoactive yellow protein mutant M100L, *Biochemistry 41*, 1915−1922.
7. Imamoto, Y., Kamikubo, H., Harigai, M., Shimizu, N., and Kataoka, M. (2002) Light-induced global conformational change of photoactive yellow protein in solution, *Biochemistry 41*, 13595−13601.
8. Lee, B.-C., Croonquist, P. A., Sosnick, T. R., and Hoff, W. D. (2001) PAS domain receptor photoactive yellow protein is converted to a molten globule state upon activation, *J. Biol. Chem. 276*, 20821−20823.
9. Xie, A. H., Kelemen, L., Hendriks, J., White, B. J., Hellingwerf, K. J., and Hoff, W. (2001) Formation of a new buried charge drives a large-amplitude protein quake in photoreceptor activation, *Biochemistry 40*, 1510−1517.
10. Brudler, R., Rammelsberg, R., Woo, T. T., Getzoff, E. D., and Gerwert, K. (2001) Structure of the I1 early intermediate of photoactive yellow protein by FTIR spectroscopy, *Nat. Struct. Biol. 8*, 265−270.
11. Meyer, T. E., Tollin, G., Hazzard, J. H., and Cusanovich, M. A. (1989) Photoactive yellow protein from the purple phototrophic bacterium, *Ectothiorhodospira halophila*−quantum yield of photobleaching and effects of temperature, alcohols, glycerol, and sucrose on kinetics of photobleaching and recovery, *Biophys. J. 56*, 559−564.
12. Hendriks, J., Gensch, T., Hviid, L., van der Horst, M. A., Hellingwerf, K. J., and van Thor, J. J. (2002) Transient exposure of hydrophobic surface in the photoactive yellow protein monitored with Nile red, *Biophys. J. 82*, 1632−1643.
13. Borucki, B., Devanathan, S., Otto, H., Cusanovich, M. A., Tollin, G., and Heyn, M. P. (2002) Kinetics of proton uptake and dye binding by photoactive yellow protein in wild type and in the E46Q and E46A mutants, *Biochemistry 41*, 10026−10037.
14. Borgstahl, G. E. O., Williams, D. R., and Getzoff, E. D. (1995) 1.4 Angstrom structure of photoactive yellow protein, a cytosolic photoreceptor: unusual fold, active-site, and chromophore, *Biochemistry 34*, 6278−6287.
15. Dux, P., Rubinstenn, G., Vuister, G. W., Boelens, R., Mulder, F. A. A., Hard, K., Hoff, W. D., Kroon, A. R., Crielaard, W., Hellingwerf, K. J., and Kaptein, R. (1998) Solution structure and backbone dynamics of the photoactive yellow protein, *Biochemistry 37*, 12689−12699.
16. Genick, U. K., Borgstahl, G. E. O., Ng, K., Ren, Z., Pradervand, C., Burke, P. M., Srajer, V., Teng, T. Y., Schildkamp, W., McRee, D. E., Moffat, K., and Getzoff, E. D. (1997) Structure of a protein photocycle intermediate by millisecond time-resolved crystallography, *Science 275*, 1471−1475.
17. Rajagopal, S., Anderson, S., Srajer, V., Schmidt, M., Pahl, R., and Moffat, K. (2005) A structural pathway for signalling in the E46Q mutant of photoactive yellow protein, *Structure 13*, 55−63.
18. Ihee, H., Rajagopal, S., Ŝrajer, V., Pahl, R., Anderson, S., Schmidt, M., Schotte, F., Anfinrud, P. A., Wulff, M., and Moffat, K. (2005) Visualizing reaction pathways in photoactive yellow protein from nanoseconds to seconds, *Proc. Natl. Acad. Sci. U.S.A. 102*, 7145−7150.
19. Schmidt, M., Pahl, R., Ŝrajer, V., Anderson, S., Ren, Z., Ihee, H., Rajagopal, S., and Moffat, K. (2004) Protein kinetics: structures of intermediates and reaction mechanism from time-resolved X-ray data, *Proc. Natl. Acad. Sci. U.S.A. 101*, 4799−4804.
20. Anderson, S., Crosson, S., and Moffat, K. (2004) Short hydrogen bonds in photoactive yellow protein, *Acta Crystallogr. D60*, 1008−1016.
21. Anderson, S., Ŝrajer, V., Pahl, R., Rajagopal, S., Schotte, F., Anfinrud, P., Wulff, M., and Moffat, K. (2004) Chromophore conformation and evolution of tertiary structural changes in photoactive yellow protein, *Structure 12*, 1039−1045.
22. Getzoff, E. D., Gutwin, K. N., and Genick, U. K. (2003) Anticipatory active-site motions and chromophore distortion prime photoreceptor PYP for light activation, *Nat. Struct. Biol. 10*, 663−668.
23. Borucki, B., Otto, H., Joshi, C. P., Gasperi, C., Cusanovich, M. A., Devanathan, S., Tollin, G., and Heyn, M. P. (2003) pH Dependence of the photocycle kinetics of E46Q mutant of photoactive yellow protein: protonation equilibrium between $I_1$ and $I_2$ intermediates, chromophore deprotonation by hydroxyl uptake, and protonation relaxation of the dark state, *Biochemistry 42*, 8780−8790.
24. Hendriks, J., van Stokkum, I. H. M., and Hellingwerf, K. J. (2003) Deuterium isotope effects in the photocycle transitions of the photoactive yellow protein, *Biophys. J. 84*, 1180−1191.
25. Imamoto, Y., Harigai, M., and Kataoka, M. (2004) Direct observation of the pH-dependent equilibrium between L-like and M intermediates of photoactive yellow protein, *FEBS Lett. 577*, 75−80.
26. Joshi, C. P., Borucki, B., Otto, H., Meyer, T. E., Cusanovich, M. A., and Heyn, M. P. (2005) Photoreversal kinetics of the $I_1$ and $I_2$ intermediates in the photocycle of photoactive yellow protein by double flash experiments with variable time delay, *Biochemistry 44*, 656−665.
27. Borucki, B., Kyndt, J. A., Joshi, C. P., Otto, H., Meyer, T. E., Cusanovich, M. A., and Heyn, M. P. (2005) Effect of salt and pH on the activation of photoactive yellow protein and gateway mutants Y98Q and Y98F, *Biochemistry 44*, 13650−13663.
28. Harigai, M., Imamoto, Y., Kamikubo, H., Yamazaki, Y., and Kataoka, M. (2003) Role of an N-terminal loop in the secondary structural change of photoactive yellow protein, *Biochemistry 42*, 13893−13900.
29. Harper, S. M., Neil, L. C., and Gardner, K. H. (2003) Structural basis of a phototropin light switch, *Science 301*, 1541−1544.
30. Harper, S. M., Christie, J. M., and Gardner, K. H. (2004) Disruption of the LOV-$J_\alpha$ helix interaction activates phototropin kinase activity, *Biochemistry 43*, 16184−16192.
31. Meyer, T. E., Tollin, G., Causgrove, T. P., Cheng, P., and Blankenship, R. E. (1991) Picosecond decay kinetics and quantum yield of fluorescence of the photoactive yellow protein from the halophilic purple phototrophic bacterium, *Ectothiorhodospira halophila*, *Biophys. J. 59*, 988−991.

32. Brudler, R., Meyer, T. E., Genick, U. K., Devanathan, S., Woo, T. T., Millar, D. P., Gerwert, K., Cusanovich, M. A., Tollin, G., and Getzoff, E. D. (2000) Coupling of hydrogen bonding to chromophore conformation and function in photoactive yellow protein, *Biochemistry 39*, 13478−13486.
33. Lee, B.-C., Croonquist, P. A., and Hoff, W. D. (2001) Mimic of photocycle by a protein folding reaction in photoactive yellow protein, *J. Biol. Chem. 276*, 44481−44487.
34. Gensch, T., Hendriks, J., and Hellingwerf, K. J. (2004) Tryptophan fluorescence monitors structural changes accompanying signalling state formation in the photocycle of photoactive yellow protein, *Photochem. Photobiol. Sci. 3*, 531−536.
35. Kyndt, J. A., Vanrobaeys, F., Fitch, J. C., Devreese, B. V., Meyer, T. E., Cusanovich, M. A., and Van Beeumen, J. J. (2003) Heterologous production of *Halorhodospira halophila* holophotoactive yellow protein through tandem expression of the postulated biosynthetic genes, *Biochemistry 42*, 965−970.
36. Kyndt, J. A., Hurley, J. K., Devreese, B., Meyer, T. E., Cusanovich, M. A., Tollin, G., and Van Beeumen, J. J. (2004) *Rhodobacter capsulatus* photoactive yellow protein: genetic context, spectral and kinetics characterization, and mutagenesis, *Biochemistry 43*, 1809−1820.
37. Imamoto, Y., Ito, T., Kataoka, M., and Tokunaga, F. (1995) Reconstitution of photoactive yellow protein from apoprotein and p-coumaric acid derivatives, *FEBS Lett. 374*, 157−160.
38. Borucki, B., Otto, H., Meyer, T. E., Cusanovich, M. A., and Heyn, M. P. (2005) A sensitive circular dichroism marker for the chromophore environment of photoactive yellow protein: assignment of the 307 and 318 nm bands to the n → $\pi^*$ transition of the carbonyl, *J. Phys. Chem. B 109*, 629−633.
39. Otto, H., Lamparter, T., Borucki, B., Hughes, J., and Heyn, M. P. (2003) Dimerization and inter-chromophore distance of Cph1 phytochrome from *Synechocystis*, as monitored by fluorescence homo and hetero energy transfer, *Biochemistry 42*, 5885−5895.
40. Lakowicz, J. R., (1999) *Principles of Fluorescence Spectroscopy*, 2nd ed., Kluwer Academic/Plenum Publishers, New York.
41. Van der Meer, B. W., Coker, G., III, and Chen, S.-Y. (1994) *Resonance Energy Transfer: Theory and Data*, VCH Publishers, New York.
42. Henry, E. R., and Hofrichter, J. (1992) Singular value decomposition: application to analysis of experimental data, *Methods Enzymol. 210*, 129−192.
43. Hendler, R. W., and Shrager, R. I. (1994) Deconvolutions based on singular value decomposition and pseudo inverse: a guide for beginners, *J. Biochem. Biophys. Methods 78*, 1−33.
44. Genick, U. K., Devanathan, S., Meyer, T. E., Canestrelli, I. L., Williams, E., Cusanovich, M. A., Tollin, G., and Getzoff, E. D. (1997) Active site mutants implicate key residues for control and light cycle kinetics of photoactive yellow protein, *Biochemistry 36*, 8−14.
45. Borucki, B., Otto, H., and Heyn, M.P. (1999) Reorientation of the retinylidene chromophore in the K, L, and M intermediates of bacteriorhodopsin from time-resolved linear dichroism: resolving kinetically and spectrally overlapping intermediates of chromoproteins, *J. Phys. Chem. B 103*, 6371−6383.
46. Albinsson, B., and Nordén, B. (1992) Excited-state properties of the indole chromophore. Electronic transition moment directions from linear dichroism measurements: effect of methyl and methoxy substituents, *J. Phys. Chem. 96*, 6204−6212.
47. Callis, P. R. (1997) $^1L_a$ and $^1L_b$ transitions of tryptophan: applications of theory and experimental observations to fluorescence of proteins, *Methods Enzymol. 278*, 113−150.
48. Meyer, T. E. (1985) Isolation and characterization of soluble cytochromes, ferredoxins and other chromophoric proteins from the halophilic phototrophic bacterium *Ectothiorhodospira halophila*, *Biochim. Biophys. Acta 806*, 175−183.
49. Groenhof, G., Lensink, M. F., Berendsen, H. J., Snijders, J. G., and Mark, A. E. (2002) Signal transduction in photoactive yellow protein. I. Photon absorption and the isomerization of the chromophore, *Proteins 48*, 202−211.
50. Gensch, T., Gradinaru, C. C., van Stokkum, I. H. M., Hendriks, J., Hellingwerf, K. J., and van Grondelle, R. (2002) The primary photoreaction of photoactive yellow protein (PYP): anisotropy changes and excitation wavelength dependence, *Chem. Phys. Lett. 356*, 347−354.
51. Heyn, M. P., Borucki, B., and Otto, H. (2000) Chromophore reorientation during the photocycle of bacteriorhodopsin: experimental methods and functional significance, *Biochim. Biophys. Acta 1460*, 60−74.
52. Drikos, G., and Rüppel, H. (1984) Polarized UV-absorption spectra of retinal isomers. 2. On the assignment of the low and high-energy absorption bands, *Photochem. Photobiol. 40*, 93−104.
53. Lin, S. W., and Mathies, R. A. (1989) Orientation of the protonated retinal Schiff base group in bacteriorhodopsin from absorption linear dichroism, *Biophys. J. 56*, 653−660.
54. Bernard, C., Houben, K., Derix, N. M., Marks, D., van der Horst, M. A., Hellingwerf, K. J., Boelens, R., Kaptein, R., and van Nuland, N. A. J. (2005) The solution structure of a transient photoreceptor intermediate: Δ25 photoactive yellow protein, *Structure 13*, 953−962.

BI051448L